

Experimental and numerical study of the wake deflections of scaled vertical axis wind turbine models

Huang, Ming; Sciacchitano, Andrea; Ferreira, Carlos

DOI

[10.1088/1742-6596/2505/1/012019](https://doi.org/10.1088/1742-6596/2505/1/012019)

Publication date

2023

Document Version

Final published version

Published in

Journal of Physics: Conference Series

Citation (APA)

Huang, M., Sciacchitano, A., & Ferreira, C. (2023). Experimental and numerical study of the wake deflections of scaled vertical axis wind turbine models. *Journal of Physics: Conference Series*, 2505(1), Article 012019. <https://doi.org/10.1088/1742-6596/2505/1/012019>

Important note

To cite this publication, please use the final published version (if applicable). Please check the document version above.

Copyright

Other than for strictly personal use, it is not permitted to download, forward or distribute the text or part of it, without the consent of the author(s) and/or copyright holder(s), unless the work is under an open content license such as Creative Commons.

Takedown policy

Please contact us and provide details if you believe this document breaches copyrights. We will remove access to the work immediately and investigate your claim.

PAPER • OPEN ACCESS

Experimental and numerical study of the wake deflections of scaled vertical axis wind turbine models

To cite this article: Ming Huang *et al* 2023 *J. Phys.: Conf. Ser.* **2505** 012019

View the [article online](#) for updates and enhancements.

You may also like

- [Integrated design of a semi-submersible floating vertical axis wind turbine \(VAWT\) with active blade pitch control](#)
Fons Huijs, Ebert Vlasveld, Maël Gormand et al.
- [Experimental and Computational Investigations of Vertical Axis Wind Turbine Enclosed with Flanged Diffuser](#)
G Surya Raj, N Sangeetha and M Prince
- [Numerical study on aerodynamic damping of floating vertical axis wind turbines](#)
Zhengshun Cheng, Helge Aagaard Madsen, Zhen Gao et al.



Connect with decision-makers at ECS

Accelerate sales with ECS exhibits, sponsorships, and advertising!

▶ Learn more and engage at the 244th ECS Meeting!

Experimental and numerical study of the wake deflections of scaled vertical axis wind turbine models

Ming Huang, Andrea Sciacchitano, Carlos Ferreira

Department of Flow Physics and Technology, Faculty of Aerospace Engineering, Delft University of Technology, Delft, the Netherlands

E-mail: m.huang-1@tudelft.nl

Abstract. Wake steering of vertical axis wind turbines (VAWTs) is investigated experimentally and numerically via stereoscopic particle image velocimetry and Reynolds averaged Navier-Stokes simulations. Three different blade pitch angles (-10° , 0° , 10°) of straight H-type VAWTs are adopted to deflect and deform the wake. The experimental results confirm the efficacy of blade pitching on the wake steering, and validate the simulation for both moderate and significant wake deflections. The simulation is then extended to full-scale VAWTs, exploring the wake deflection effects on the power performance of VAWT arrays. The effects of inter-turbine distances and pitching configurations are considered. With the upwind VAWT deflecting the wake, the overall power coefficient is increased by 41%.

1. Introduction

The ability to steer and deform wind turbine wakes can result in increased wind farm power density and reduced energy costs and can be used to optimise wind farm designs. The wake steering is often achieved by yawing the rotor discs of HAWTs, using an active control accounting for the variable wind direction [1, 2, 3, 4, 5, 6]. With this technique, the wind farm's total power production is estimated to increase considerably, ranging from 4% to 13%.

The ability to deflect wakes within an array of vertical axis wind turbines is of similar interest. A previous work of the authors [7] deflects the wake of VAWTs by varying the load distribution. Pitching the blades is the simplest way to modify the load. Recently, [8] measured the blade load with an in-house designed VAWT that is able to perform active pitch control continuously, showing that the blade load can be effectively modified with fixed blade pitch. A few studies can also be found in the literature on the deflection of VAWTs' wake based on pitched blades. Jadeja (2018) [9] investigated the wake deflection of a pitched VAWT using the actuator line model (ALM) together with unsteady Reynolds averaged Navier-Stokes (RANS) simulation. Guo and Lei (2020) [10] proposed to deflect the wake by effectively altering the inclination angle of the rotor blade to the flow (which is a close analogue to adjusting the nacelle inclination for a HAWT); Mendoza et al. (2019) [11] propose to achieve a similar outcome by altering the pitch of the struts connecting the blades to the drive shaft. Both of these are mechanically complex and potentially difficult to implement even in the controlled environment of wind tunnel experiments.

Hence, in the present work, wakes of lab-scale VAWTs with fixed blade pitches are measured using stereo-PIV. The measured data proves the concept of wake deflection and deformation using pitching blades and is used to validate the numerical simulation based on ALM and RANS. The simulation is then extended to a full-scale VAWT, showing promise to significantly increase the power output of VAWT farms.



2. Experimental apparatus and procedures

The experiments are conducted in the Open-Jet Facility (OJF) of the TU Delft Aerodynamics Laboratories. The OJF has a contraction ratio of 3:1 and an open exit that measures 2.85×2.85 m². The stable free-stream, which is not impacted by the development of the jet shear layer [12], develops at a semi-angle of 4.75° and creates an effective test area of approximately 2.35×2.35 m² located 3 m behind the exit. It covers the entire wake cross-sections of the VAWTs. The test wind speed is $U_\infty = 5$ m s⁻¹, and the turbulence intensity is less than 2% [13].

2.1. VAWT model

The scaled VAWT model has an H-shaped rotor with dimensions of 30×30 cm. The model's two straight blades are made of aluminium and feature NACA0012 airfoils with a chord length of 0.03 m, rotating at a constant TSR of 2.5 to keep a moderate thrust coefficient (around 0.8) for such a high solidity turbine [7]. It would be better to control the TSR dynamically based on the thrusts, however, employing active controls requires real-time measurements of the blade forces, which is out of the scope of this work. The model's solidity is 0.2. The blades are connected to the tower via a pair of struts. The cross-section profile of the struts on the blade side is NACA0012 and transitions to an ellipse with a thickness of 12% on the tower side to reduce drag and flow separation. The blades and struts are connected with two pairs of bolts that allow for quick release and adjustment of the fixed pitching angle; 3D printed adaptors are used to adjust the pitch angle (figure 1). Blade pitching towards the tower is considered positive and vice versa. The rotor is powered by a *MAXON* EC 90 flat brushless motor, which is controlled by a *ESCON* 50/5 control module. A flexible coupling is employed to filter out small vibrations and compensate for any misalignment due to machining accuracy.

2.2. PIV set up

The velocity fields in the wake of the VAWTs are obtained using stereoscopic PIV, which measures three velocity components within two-dimensional planes. An overview of the experimental setup is shown in figure 2. As illustrated, the ground effect is not accounted for in the measurement. The velocity fields in the wake of the VAWTs were measured using stereoscopic Particle Image Velocimetry (PIV), which measures three velocity components within two-dimensional planes. The PIV setup consisted of a Quantel *Evergreen* double-pulsed Nd:YAG laser that produced pulses with an energy of 200 mJ at a wavelength of 532 nm within a laser sheet that was approximately 3 mm wide. Water-glycol seeding particles with an average diameter of 1 μ m were released by a *SAFEX* smoke generator and imaged by two LaVision's Imager sCMOS cameras in successive cross-sections of the wake. The cameras had an image resolution of 2560 px \times 2160 px, a pixel pitch of 6.5 μ m/px, and were coupled with 50 mm lenses that had a numerical aperture of 4. The cameras were positioned approximately 2.2 m away from the centre of the laser sheet with a stereoscopic angle of 90° , resulting in a camera field of view (FoV) of approximately 80×55 cm², a magnification factor of 0.026, and a digital image resolution of 3.9 px/mm. The sampling frequency is 15 Hz and 400 images for each location are acquired. Detailed descriptions of the experimental apparatus can be found in the previous work [7]. To accurately position the PIV system, a traversing system was employed that enabled navigation from 0.3 m to 3 m behind the wind tunnel exit in steps of 0.3 m. Figure 2 provides an overview of the experimental setup.

2.3. Measured Cases

Measured cases are listed in table 1. As defined by Tescione et al. (2014), the near wake lasts until around $3D$ downwind of the turbine, featuring stronger tip vortices, higher turbulence and higher pressure gradients. The downwind turbine is placed $5D$ behind the upwind one, which

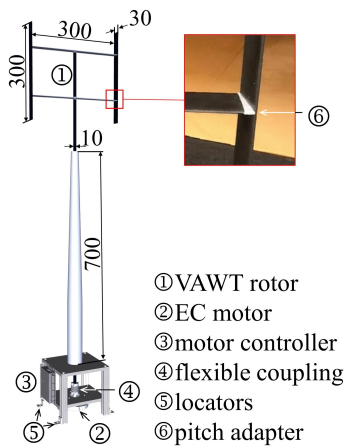


Figure 1: The VAWT model.

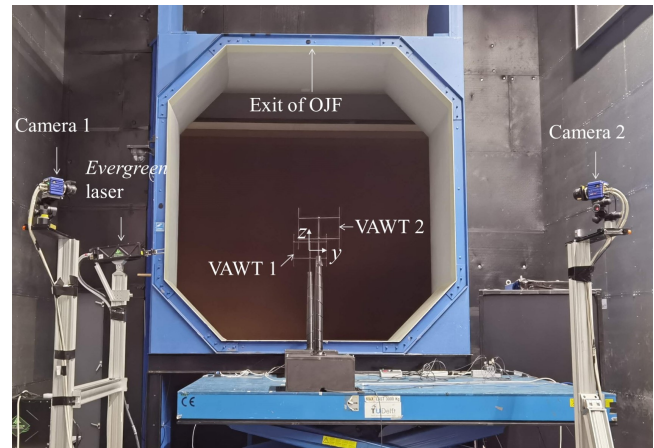


Figure 2: Experimental setup.

is in the far wake region, to focus on the effects of deflected velocity deficit on the downwind turbine's performance.

Table 1: Description of the measured configurations.

	case	Description
Isolated VAWTs	P-10	Isolated VAWT with pitched blades, -10°
	P0	Isolated VAWT with zero pitch
	P10	Isolated VAWT with pitched blades, $+10^\circ$
VAWTs in tandem	P-10_0D	VAWT1 with -10° pitch, VAWT2 with zero transverse offset
	P0_0D	VAWT1 with zero pitch, VAWT2 with zero transverse offset
	P10_0D	VAWT1 with 10° pitch, VAWT2 with zero transverse offset

3. Numerical simulation approach

3.1. Actuator line model

The ALM is based on a blade element approach combined with two-dimensional airfoil characteristics. It determines the blade loading applied to the flow field iteratively using the local angle of attack and a lookup table of the airfoil's static force coefficients. The ALM can be augmented with correction models for blade loading that account for phenomena not captured by a static lift-drag polar diagram, such as dynamic stall models for unsteady airfoil behaviour and end-effect models for three-dimensional blade tip losses. The ALM has been widely used and validated in previous studies [14, 15, 16].

The present work uses the ALM with an unsteady Reynolds-averaged Navier-Stokes (RANS) solver (*pimpleFoam* library from OpenFOAM) and an open source library called *turbinesFoam* (mainly developed by Bachant, 2016 [17]). The $k - \epsilon$ turbulence model has been tuned for the turbulence intensity level and Reynolds number adopted in this work, as documented in the Master thesis of Monni [18]. Some comparisons and convergence studies for meshes and time steps have been reported in previous work [18, 19, 20].

3.2. Cases simulated

3.2.1. Lab-scale VAWT The cases of moderate and strong wake deflections of the isolated lab-scale VAWTs (P0 and P10, respectively) are simulated, to validate the numerical method.

3.2.2. Up-scaled VAWT The attributes of the Up-scaled VAWT and the inflow are listed in table 2. The chord-based Reynolds number is around 1×10^7 . The blade airfoil features a high stall angle in such a high Reynolds number allowing for an extensive operation range for the blade pitching angle without hampering the performance. Contrary to the experimental cases, the VAWT simulated are with low solidity. Therefore, the tip speed ratio of the up-scaled simulation is set to a relatively high value (4.5) while the overall thrust is remained, thus avoiding severe dynamic stalls of the rotating blades. For the sake of simplicity, struts, tower and floor are not present in the simulation, and the freestream is uniform.

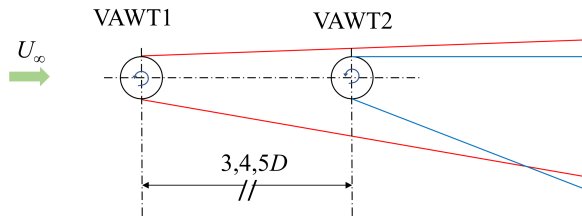


Figure 3: A schematic top view of array configurations.

Three groups of cases are analysed, covering the isolated VAWTs and arrays with two VAWTs (figure 3): 1) First, the wakes of isolated VAWTs are simulated, with different fixed blade pitches (-10° , 0° and 10°) to deflect the wake. The attributes of the VAWT and the freestream are listed in table 2. It is noted that the rotation speed of all the turbines is kept the same unless otherwise stated, resulting in a tip speed ratio of 4.5 with respect to the freestream. 2) Then, the inter-turbine distance effects on wake interactions are studied. Two VAWTs are considered and the first turbine deflects the wake via different blade pitch angles while the second one operates with zero pitch angle. The inter-turbine distance varies between 3, 4 and 5 rotor diameters. 3) To shed light on optimum blade pitch patterns for two pitched VAWTs, the third group of simulations has been conducted where VAWT1 and VAWT2 are both pitched to deflect their wakes; The inter-turbine distance is four diameters.

Table 2: Attributes of the simulated up-scaled VAWT and the freestream.

Symbol	Parameter	Value
U_∞	Freestream velocity	10 m s^{-1}
I	Turbulence intensity	8%
AR	Aspect ratio, H/D	1
Re_D	Diameter-based Reynolds number	1.1×10^8
B	Number of blades	3
c/R	Normalised chord length	0.025
λ	Tip speed ratio	4.5
φ	Pitch angles	$-10^\circ, 0^\circ, 10^\circ$
	Blade profile	NACA0025
	Rotation direction	Counterclockwise

4. Results and discussion

4.1. Experimental results

Isolated lab-scale VAWTs

The velocity, vorticity and turbulence intensity fields in the wake of isolated VAWTs are illustrated in figure 4. Data at different downwind locations is available in the previous work [7]. It is observed that different pitching angles result in different streamwise vorticity systems, and thus deflect and deform the wake differently. The wake is deflected slightly when the pitch angle is 0° because the differences in perceived wind speed between the advancing and retreating sides are non-negligible at $\text{TSR} = 2.5$. Such differences in the inflow produce different forces laterally, deflecting the wake.

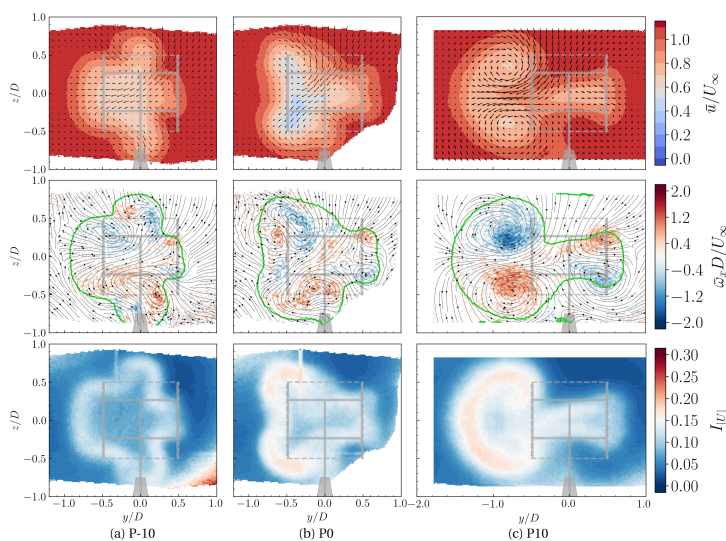


Figure 4: Contours of streamwise velocity with in-plane velocity vectors, vorticity with in-plane streamlines, and turbulence intensity for the isolated VAWT P-10, P0 and P10 at $x_1/D = 5$. Green contour lines are where $\bar{u}/U_\infty = 1$, showing the outline of the wake; Grey schematics denote the transverse location and frontal area of VAWT1.

Lab-scale VAWT arrays

An overview of the placement of the VAWTs and measured velocity contours are given in figure 5. Compared to the isolated turbines, the wakes of the inline cases remain similar to those of the isolated VAWTs at $x/D \geq 5$, but the velocity deficits in the wake centre are increased due to the presence of VAWT2. P-10_0D features a deeper velocity deficit than P0_0D, because the former exerts a higher thrust against the free-stream while the lateral forces of the two are similar [7]. In contrast, P10_0D imparts the lowest velocity deficit. This is due to two reasons: first, a large portion of the extracted streamwise momentum is transferred to the horizontal deflection, and that explains the largest wake deflection compared with the other two cases; Second, its significant wake deformation yields a faster recovery, by enhancing the entrainment of momentum via the advection and the increased wake-free-stream interface [7].

4.2. Simulation validation based on lab-scale VAWTs

Velocity deficit profiles in the horizontal and vertical cross-sections crossing the centre of the lab-scale VAWT are compared to validate the simulation. Both moderate and significant wake deflections are examined. For moderate deflection (P0), as illustrated in figure 6, the simulation matches greatly with the experiment in the near wake and produces comparable velocity deficit and wake deflection in the far wake. For P10 (figure 7), the curves of the simulation and the experiment collapse since $x/D = 2$. The slight difference at $x/D = 1$ could be attributed to the dynamic stall correction adopted in the simulation, which underestimates the lift coefficient at an extremely large angle of attack and low Reynolds number.

As illustrated in figure 8, the simulated and measured velocity contours in P0 and P10 are compared. The cross-sections at both near and far regions in the wake ($x/D = 1, 5, 10$)

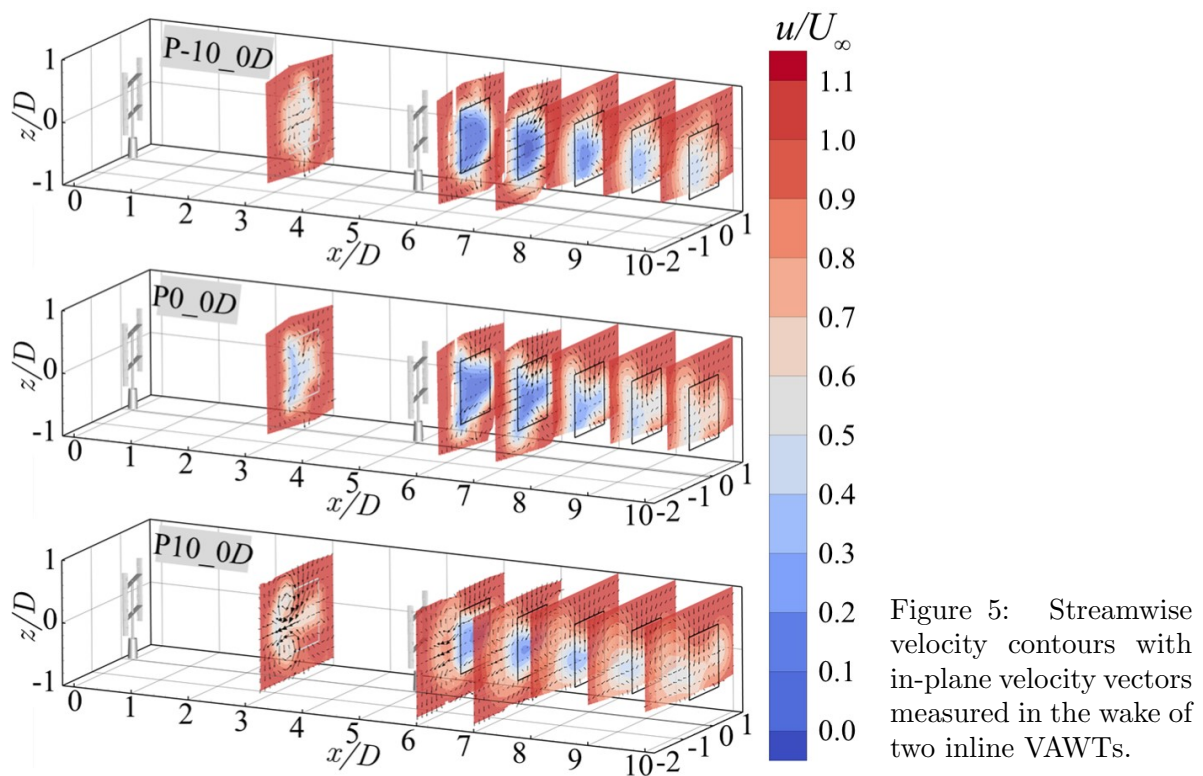


Figure 5: Streamwise velocity contours with in-plane velocity vectors measured in the wake of two inline VAWTs.

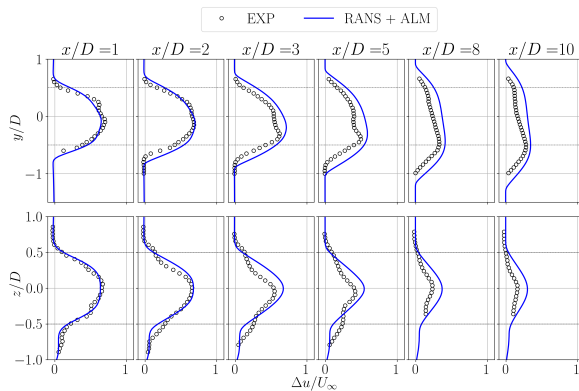


Figure 6: Profiles of centre-line velocity deficit of P0 for moderate wake deflection.

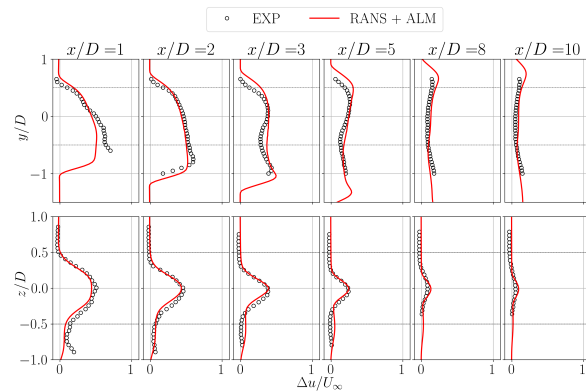


Figure 7: Profiles of centre-line velocity deficit of P10 for significant wake deflection.

are compared. For P0, the velocity deficits and deflection match well, whereas the wake shapes are deformed slightly differently. This could be attributed to inaccurate blade loading determination under such low Re and low TSR scheme. In contrast, for P10, the simulation resolves the wake deflection and deformation, the in-plane motions and the vortex locations. The simulation performs excellently in the far wake ($x/D = 5, 10$), producing velocity fields resembling the experimental data. In the near wake, it underestimates the maximum deficit around the windward (also the advancing) side of the VAWT.

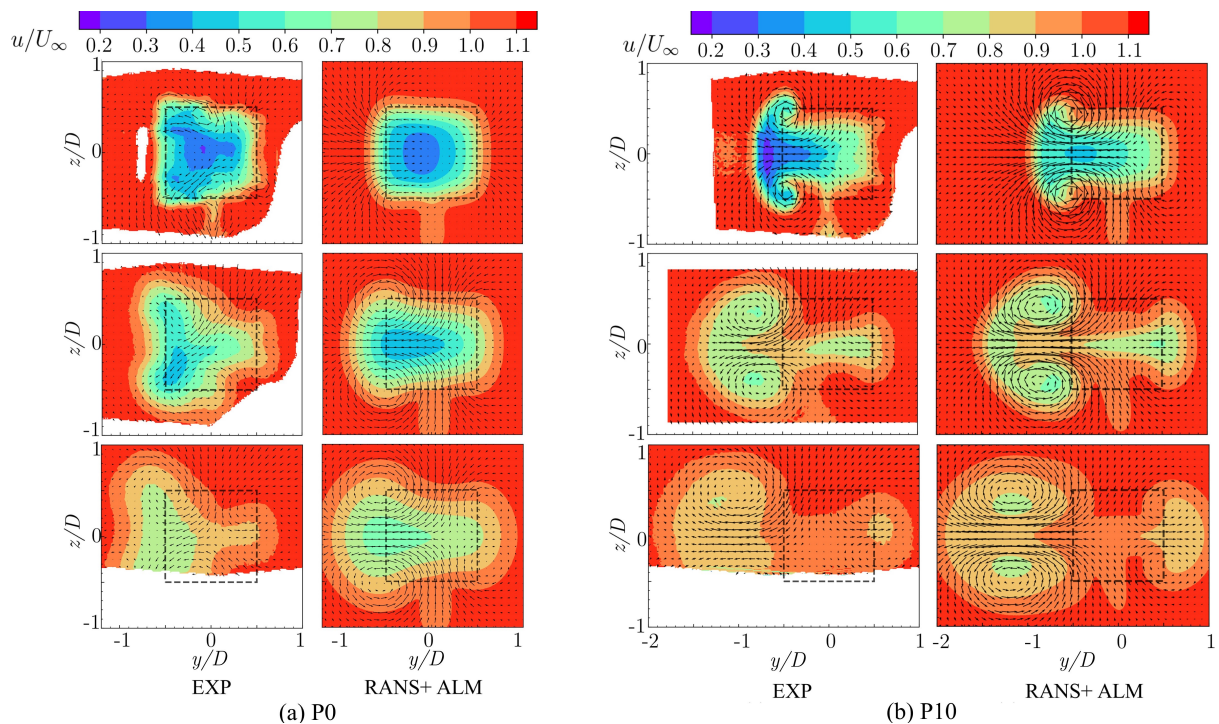


Figure 8: Comparison of cross-sectional streamwise velocity contours with in-plane velocity vectors of P0 and P10. Black squares denote the frontal area of the VAWT. Each row from top to bottom are extracted at $x/D = 1, 5, 10$, respectively.

4.3. Simulation results

Isolated up-scaled VAWTs

The streamwise velocity and vorticity fields of the isolated VAWTs are presented in figure 9 and 10, respectively. P-10 deflects the wake towards the leeward of the swept area and P10 towards the windward. The wake of P-10 and P10 features vertical and horizontal stretching, respectively; Both the deflection and the stretching contribute to a higher streamwise velocity in the projected area at the far wake ($x/D = 5$) compared to P0, and thus a higher available wind power [7].

The available power (AP) in the wakes of the isolated VAWTs is calculated based on the approach introduced in [7], and is illustrated in figure 11. P-10 and P10 increase the AP remarkably compare to P0, e.g., at $x/D = 5$, AP of the former recovers to more than 0.75 while the AP of P0 only reaches 0.34. On the other hand, the minimum AP of P-10 and P0 remains around $y_0/D = 0$; whereas P10 deflect the minimum AP horizontally, and it reaches $y_0/D = 1.2$ at $x/D = 9$. It is observed that the wake of P-10 features the highest AP off the inline position, which indicates closer deployment spaces abreast.

Up-scaled VAWT Arrays

4.3.1. Turbine performances The performances of the VAWT arrays are listed in table 3. The coefficients are calculated based on the freestream velocity instead of the inflow velocity of each turbine, for the sake of a direct comparison of the absolute value of the power extraction.

The wake deflection significantly increases the overall power extraction of the VAWT array by 30% to 41% compared to the cases without deflection, which proves the prediction in [7]. For all the cases in table 3, as the inter-turbine distance increases, the performance of VAWT2 first increases notably and then converges to a constant. It is because the wake recovery rate

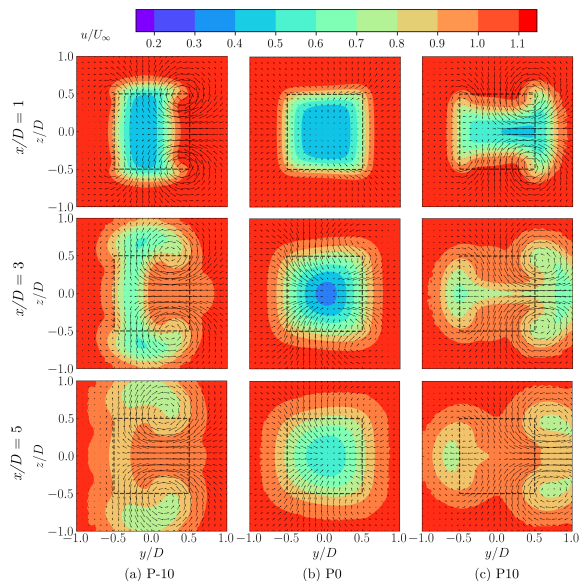


Figure 9: Streamwise velocity contours and in-plane vectors. Black dashed squares denote the VAWT's frontal area.

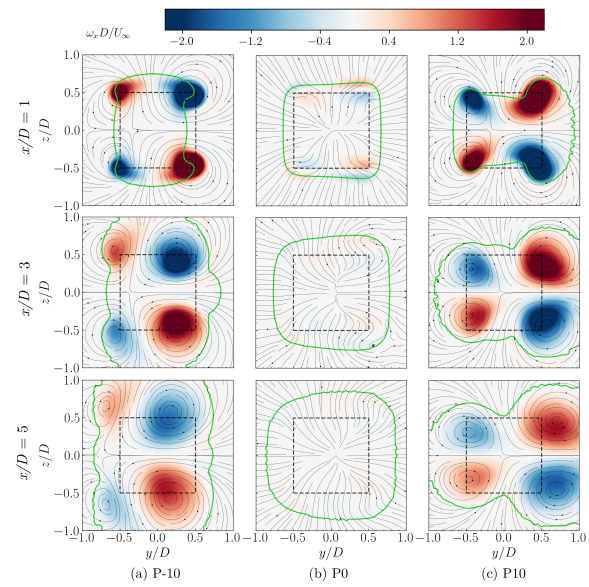


Figure 10: Streamwise vorticity contour and in-plane streamlines. Black dashed squares denote the VAWT's frontal area.

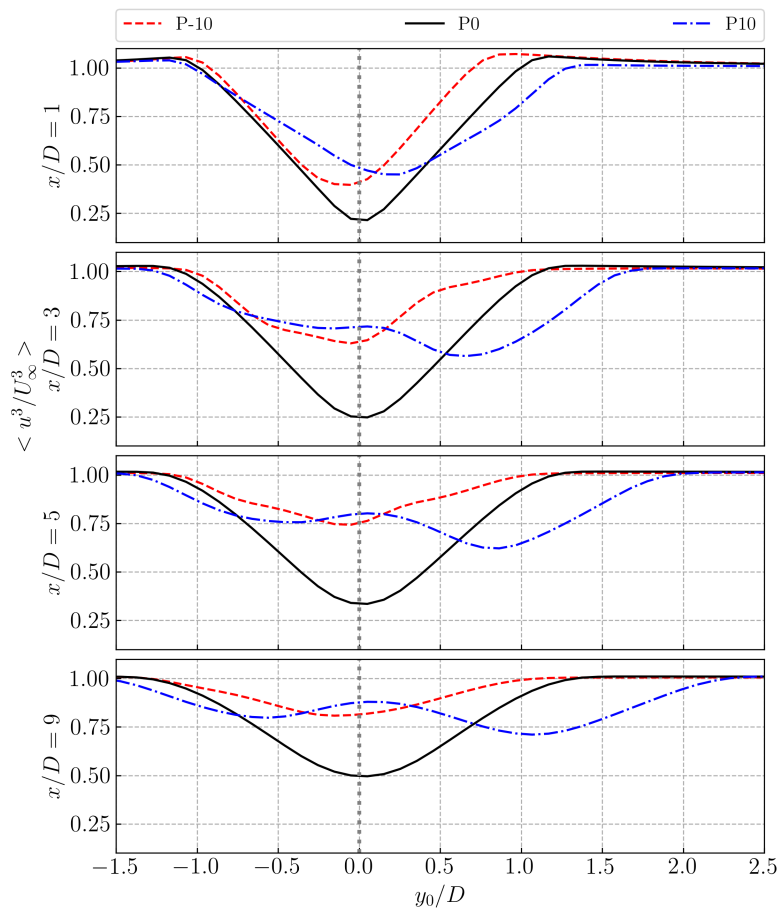


Figure 11: Available power behind the isolated VAWTs.

in the far wake is slow compared to that in the near wake. Thus, once VAWT2 is placed in the far wake of VAWT1, the available power increment by increasing inter-turbine distance is not as effective as in the near wake. As demonstrated in [7], the momentum recovers faster in the near wake due to streamwise vorticity that enhances the advection. While in the far wake, the turbulent transport of momentum takes the lead, which is less effective than the advection. It is interesting that when the two VAWTs are placed close ($3D$), the power coefficient of the upwind turbine drops slightly; while increasing the inter-turbine distances, the downwind turbine does not affect the upwind one anymore.

On the other hand, when the inter-turbine distance is kept constant, and both turbines are pitched to deflect the wake (table 4), the overall power output still mainly depends on the performance of VAWT2. Among these cases, P-10_P10 yields the highest $C_{P,total}$ while leaving the most substantial velocity deficit region within the projected area, hampering the performance of downwind turbines in line with VAWT2. In contrast, the combination of two P-10 (i.e. P-10_P-10) might be a better balance, of which the wake further downstream is effectively deflected [21] while the overall performance is increased by +20%.

Table 3: Performance of two VAWTs placed aligned, with an inter-turbine distance of 3,4 and 5*D*. VAWT1 is pitched with different angles, while VAWT2 has zero blade pitch angle. Coefficients are calculated based on U_∞ . Differences compared to P0_{3,4,5}*D* are marked in red.

Case	C_{P1}	$C_{T,x1}$	$C_{T,y1}$	C_{P2}	$C_{T,x2}$	$C_{T,y2}$	$C_{P,total}$
P-10_3 <i>D</i>	0.45	0.69	-0.37	0.35 (+289%)	0.55	0.07	0.80 (+38%)
P0_3 <i>D</i>	0.49	0.67	0.02	0.09	0.32	0.00	0.58
P10_3 <i>D</i>	0.44	0.64	0.34	0.38 (+322%)	0.59	-0.06	0.82 (+41%)
P-10_4 <i>D</i>	0.46	0.69	-0.37	0.40 (+167%)	0.61	0.08	0.86 (+32%)
P0_4 <i>D</i>	0.50	0.68	0.02	0.15	0.39	0.00	0.65
P10_4 <i>D</i>	0.44	0.64	0.34	0.41 (+173%)	0.61	-0.04	0.85 (+30%)
P-10_5 <i>D</i>	0.46	0.69	-0.37	0.43 (+169%)	0.63	0.08	0.89 (+35%)
P0_5 <i>D</i>	0.50	0.68	0.02	0.16	0.41	0.00	0.66
P10_5 <i>D</i>	0.44	0.64	0.34	0.43 (+169%)	0.63	-0.03	0.87 (+32%)

Table 4: Performance of two pitched VAWTs placed aligned, with an inter-turbine distance of 4*D*. Coefficients calculated based on U_∞ . Differences compared to P0_4*D* are marked in red.

Case	C_{P1}	$C_{T,x1}$	$C_{T,y1}$	C_{P2}	$C_{T,x2}$	$C_{T,y2}$	$C_{P,total}$
P0_P0(P0_4 <i>D</i>)	0.50	0.68	0.02	0.15	0.39	0.00	0.65
P0_P-10	0.50	0.68	0.02	0.11 (-27%)	0.4	-0.27	0.61 (-6%)
P0_P10	0.49	0.68	0.02	0.06 (-60%)	0.35	0.19	0.55 (-15%)
P-10_P-10	0.45	0.69	-0.37	0.33 (+120%)	0.67	-0.27	0.78 (+20%)
P-10_P10	0.46	0.69	-0.37	0.35 (+133%)	0.51	0.35	0.81 (+25%)
P10_P-10	0.44	0.64	0.34	0.31 (+107%)	0.62	0.23	0.75 (+15%)
P10_P10	0.44	0.64	0.34	0.31 (+107%)	0.62	0.23	0.75 (+15%)

5. Conclusions

The performance and wake aerodynamics of lab-scale and up-scaled VAWTs have been measured and simulated. The measurement results validate the simulation. The simulation confirms the efficacy of wake deflection using blade pitches; Other main findings are as follows:

- The concept of VAWT wakes deflection using fixed blade pitch has been proved. By blade pitching, the velocity deficit and vorticity system in the wake are modified significantly, whereas the power performance decreases slightly.
- Wake deflection of the upwind VAWT has a significant impact on the performances of downwind VAWTs. It increases the overall power output by 15-41% in the VAWT array simulated in this work.
- Judging by the AP distribution, the wake of pitched VAWT arrays in the present work feature quicker momentum recovery. This is attributed to enhanced momentum influxes produced by the vortex structure.

References

- [1] Fleming P, Annoni J, Shah J J, Wang L, Ananthan S, Zhang Z, Hutchings K, Wang P, Chen W and Chen L 2017 *Wind Energy Science* **2** 229–239
- [2] Fleming P, King J, Dykes K, Simley E, Roadman J, Scholbrock A, Murphy P, Lundquist J K, Moriarty P, Fleming K, van Dam J, Bay C, Mudafort R, Lopez H, Skopek J, Scott M, Ryan B, Guernsey C and Brake D 2019 *Wind Energy Science* **4** 273–285
- [3] Park J and Law K H 2015 *Energy Conversion and Management* **101** 295–316
- [4] Boersma S, Doekemeijer B M, Gebraad P M, Fleming P A, Annoni J, Scholbrock A K, Frederik J A and Van Wingerden J W 2017 *Proceedings of the American Control Conference* 1–18
- [5] Bastankhah M and Porté-Agel F 2019 *Journal of Renewable and Sustainable Energy* **11** 023301
- [6] Howland M F, Lele S K and Dabiri J O 2019 *Proceedings of the National Academy of Sciences of the United States of America* **116** 14495–14500
- [7] Huang M, Sciacchitano A and Ferreira C 2023 *Wind Energy*
- [8] LeBlanc B and Ferreira C 2021 *Wind Energy*
- [9] Jadeja A 2018 *Wake Deflection Technique for Vertical Axis Wind Turbines using Actuator Line Model in OpenFOAM* Master's thesis Delft University of Technology
- [10] Guo J and Lei L 2020 *Energies* **2020**, Vol. 13, Page 6281 **13** 6281
- [11] Mendoza V and Goude A 2019 *Wind Energy* **22** 538–546
- [12] Lignarolo L E M, Ragni D, Krishnaswami C, Chen Q, Simão Ferreira C J, Van Bussel G J W, Ferreira C J S and Van Bussel G J W 2014 *Renewable Energy* **70** 31–46
- [13] Lignarolo L E, Ragni D, Scarano F, Simão Ferreira C J and Van Bussel G J 2015 *Journal of Fluid Mechanics* **781** 467–493
- [14] Sørensen J N and Shen W Z 2002 *Journal of Fluids Engineering, Transactions of the ASME* **124** 393–399
- [15] Troldborg N 2008 *Actuator Line Modeling of Wind Turbine Wakes* Ph.D. thesis Technical University of Denmark
- [16] Sarlak H, Meneveau C and Sørensen J N 2015 *Renewable Energy* **77** 386–399
- [17] Bachant P, Goude A and Wosnik M 2016 *arXiv preprint* 1–21 (*Preprint* 1605.01449)
- [18] Monni D 2021 *Numerical simulating and analytical modelling the wake behind vertical axis wind turbines: a verification analysis* Master's thesis Politecnico di Torino
- [19] Patil Y V 2021 *PIV Experimental Comparison of Vertical Axis Wind Turbine Wake with Theoretical Models* Master's thesis Delft University of Technology
- [20] Nikhilesh K V 2021 *Simulation and validation of wake deflection in vertical-axis wind turbines* Master's thesis Delft University of Technology
- [21] Huang M 2023 *Wake and Wind Farm Aerodynamics of Vertical Axis Wind Turbines* Ph.D. thesis Delft University of Technology